

Modeling of Modulated Exosome Release from Differentiated Induced Neural Stem Cells for Targeted Drug Delivery

Mladen Veletić, Michael Taynnan Barros, *Member, IEEE*, Hamidreza Arjmandi, Sasitharan Balasubramaniam, *Senior Member, IEEE*, and Ilangko Balasingham, *Senior Member, IEEE*

Abstract—A novel implantable and externally controllable stem-cell-based platform for the treatment of Glioblastoma brain cancer has been proposed to bring hope to patients who suffer from this devastating cancer type. Induced Neural Stem Cells (iNSCs), known to have potent therapeutic effects through exosomes-based molecular communication, play a pivotal role in this platform. Transplanted iNSCs demonstrate long-term survival and differentiation into neurons and glia which then fully functionally integrate with the existing neural network. Recent studies have shown that specific types of calcium channels in differentiated neurons and astrocytes are inhibited or activated upon cell depolarization leading to the increased intracellular calcium concentration levels which, in turn, interact with mobilization of multivesicular bodies and exosomal release. In order to provide a platform towards treating brain cancer with the optimum therapy dosage, we propose mathematical models to compute the therapeutic exosomal release rate that is modulated by cell stimulation patterns applied from the external wearable device. This study serves as an initial and required step in the evaluation of controlled exosomal secretion and release via induced stimulation with electromagnetic, optical and/or ultrasonic waves.

Index Terms—Brain, Drug Delivery Systems, Exosomes, Glioblastoma, Molecular Communication, Stem Cells.

I. INTRODUCTION

Glioblastoma Multiforme is the most prevalent and devastating brain disease whose treatment has the lowest success rates compared to other therapeutic cancer technologies [1]. The development of brain drug delivery systems for this type of cancer is very challenging because of side effects, the complexity of the structures of the brain, and the stringent Blood-Brain Barrier (BBB) that protects the brain

M. Veletić is with the Intervention Centre, Oslo University Hospital (OUS), 0372 Oslo, Norway, and the Faculty of Electrical Engineering, University of Banja Luka, 78000 Banja Luka, Bosnia and Herzegovina (e-mail: mlavel@rr-research.no).

M. T. Barros is with the BioMediTech Institute, Tampere University, 33520 Tampere, Finland and the TSSG, Waterford Institute of Technology, X91 P20H Waterford, Ireland (e-mail: michael.barros@tuni.fi).

H. Arjmandi is with the Electrical Department, Yazd University, Yazd, Iran, and the Department of Electronics and Telecommunications, Norwegian University of Science and Technology (NTNU), 7491 Trondheim, Norway (e-mail: hamidreza.arjmandi@ntnu.no).

S. Balasubramaniam is with the Telecommunication Software and Systems Group, Waterford Institute of Technology, X91 P20H Waterford, Ireland (e-mail: sasib@tssg.org).

I. Balasingham is with the Intervention Center, Oslo University Hospital (OUS), 0372 Oslo, Norway, and with the Department of Electronics and Telecommunications, Norwegian University of Science and Technology (NTNU), 7491 Trondheim, Norway (e-mail: ilangko.balasingham@ntnu.no).

from damage and potentially toxic blood-borne molecules. Besides, the lack of efficient technologies to deliver drugs in the located deep and functional brain regions, such as the *brain parenchyma*, and across the BBB hinders the treatment of brain pathologies [2]. Hence, novel technologies for Glioblastoma cancer therapy must emerge to overcome the BBB blockage while efficiently reaching the brain parenchyma within safety guidelines.

Molecular communication paradigm has been recently proposed to model particulate drug delivery systems, e.g., [3], [4], [5], [6] and yield analytical expressions that can be of practical use. An **externally controllable molecular communication platform** [7] that consists of stem cells acting as therapeutic, reporting and diagnostic bio-nanomachines has been proposed in the project GLADIATOR: *Next-generation Theranostics of Brain Pathologies with Autonomous Externally Controllable Nanonetworks: a Trans-disciplinary Approach with Bio-nanodevice Interfaces* (EU-H2020-FET-Open #828837). The project is focused on Glioblastoma treatment based on stem-cell-based treatment and external control of bio-nanomachines communications and comprises of the following [8]:

- The *therapeutic bio-nanomachines* – autologous organoids of engineered induced Reprogramming Neural Stem Cells (iR-NSCs) implanted into the brain parenchyma to synthesize and release rationally designed therapeutic molecules. The iR-NSCs are controlled by external miniature wearable devices via in-messaging communication channels. Therapeutic molecules interfere with the target Glioblastoma cells whose location is known. Therapeutic molecules also interfere with another type of bio-nanomachines, that we call reporting bio-nanomachines.
- The *reporting bio-nanomachines* – engineered Glioblastoma Stem Cells (GSCs) that serve as the gateway for communicating the efficacy of the treatment. The GSCs synthesize and release reporting molecules.
- The *diagnostic bio-nanomachines* – engineered induced Monitoring Neural Stem Cells (iM-NSCs) that collect and analyze reporting molecules. The iM-NSCs serve as ‘sensors’ of the hybrid implantable diagnostic system which provides feedback to external miniature wearable devices via out-messaging communication channels.

External wearable devices with enabling communication interfaces, iR-NSCs, GSCs, and iM-NSCs form a radically new

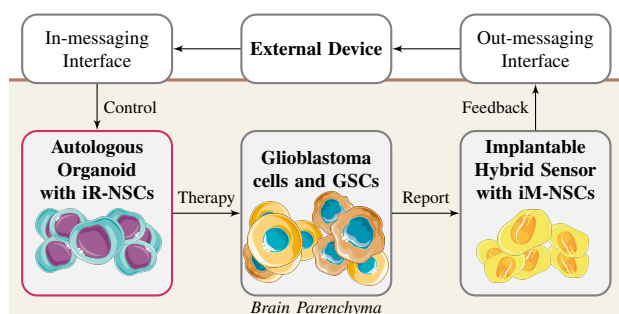


Fig. 1. Block diagram of the brain tumor management platform as a fully autonomous externally controllable molecular communication network. The controlled release of therapeutic molecules by the autologous organoid has been considered in the presented paper.

closed-loop platform for the management of brain malignancies shown in Fig. 1, and provide a breakthrough theranostic (therapeutic + diagnostic) intervention.

A promising strategy in stem-cell based platforms is to use extracellular vesicles, specifically **exosomes**, as cargos to deliver, respectively, therapeutic and reporting molecules to their recipients [9], [10], [11]. Exosomes are 40 – 100 nm cell-derived extracellular vesicles that play an important role in cell-to-cell signaling by keeping and transporting transmembrane proteins in their lipid bilayer and the cytosol molecular components from their progenitor cell including functional proteins, genetic lipids, genetic materials like messenger RNA (mRNA), microRNA (miRNA), short interfering RNA (siRNA), and genomic DNA (gDNA) [9]. Upon arrival to the target cell, exosomes fuse to the cell's membrane and deliver the transmembrane proteins and biologically active molecules. Due to their biological tolerability, natural targeting, and phagocytosis-inhibition factors, exosomes have been recently regarded as one of the most promising opportunities to deliver chemical packages to the target cell, while protecting the packages from enzymes circulating in body fluids [12]. Hence, exosomes are envisioned to pose as the main carrier to deliver reactive drug molecules to Glioblastoma cells within a potential therapeutic solution termed as an **exosome-mediated drug delivery system** [13]. Of note, a therapeutic combination of proteins, lipids and genetic materials assembled in exosomes for the treatment of Glioblastoma is unknown at present and represents an open research question.

The therapeutic bio-nanomachines, i.e., the iR-NSCs which synthesize and release exosomes, can be obtained from human somatic cells through direct lineage conversion of differentiated cells [14]. The iR-NSCs implanted into the brain differentiate into *neurons* and *glia*. In the adult mouse brain though, they have demonstrated long-term survival and differentiation into neurons (cortex: 3.26% ± 2.14%; hilus: 2.51% ± 1.11%, observed in 6 mice), astrocytes (cortex: 74.46% ± 5.38%; hilus: 68.87% ± 4.48%, observed in more than 5 mice), and oligodendrocytes (cortex: 4.34% ± 2.20%; hilus: 4.24% ± 2.03%, observed in more than 3 mice) within six months [15]. Differentiated iR-NSCs migrate, functionally integrate, and interact with the existing neuronal circuitry. The therapeutic exosomes are produced through intracellular machinery and

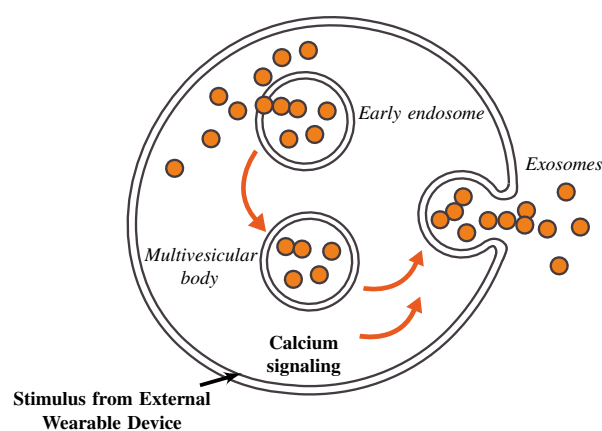


Fig. 2. Exosome biogenesis and release from the late endosomes known as the multivesicular bodies. Extracellular stimuli can enhance exosome formation and trigger exosome release.

released from cells upon fusion of an intermediate endocytic compartment, called the multivesicular body, with the plasma membrane through the process called exocytosis [16], as shown in Fig. 2.

There is the experimental evidence in the literature that exosome release from neurons and glia within the central nervous system does exist in-vitro [17] and in-vivo [18], [19], [20], [21], [22], [23]. Besides, the experimental evidence shows that 1) in neurons, glutamatergic activity is enhanced by *depolarization* and an increase in the *intracellular calcium* which is further associated with enhanced exosomal secretion and release from somato-dendritic compartments [24], [25], and 2) in astrocytes, vesicular secretion and release are regulated by *intracellular calcium* levels [26], [27]. Although the exact molecular mechanisms underlying regulated exocytosis in neurons and astrocytes have yet to be fully resolved, we form a hypothesis based on the cited works that *stimulation patterns, e.g., radio-frequency, ultrasonic, or optical waves* [28], [29], [30], *applied from the external wearable device to neurons and astrocytes, depolarize their membranes and change intracellular calcium dynamics which can be further associated with alteration in exosomal release*. Here we aim to theoretically investigate the aspects of controlled therapeutic exosomal release by computing the modulated release rate and the concentration of released exosomes from a proposed mathematical model that combines the i) cell depolarization, ii) intracellular calcium signaling, and iii) vesicular exocytosis. The proposed model is first-of-a-kind and distant from the existing scarce computational models regarding exosomes mostly developed to study the role of exosome communication in the cancer-immunity interplay [31], [32]. Of note, mechanisms associated with biogenesis of therapeutic exosomes with Glioblastoma targeting ligands and modification of the cell membranes with promoters sensitive to specific wavelengths in the electromagnetic spectrum are beyond the scope of this paper.

The presented paper contributes by enabling computation of the modulated exosomal release rates that are required within the proposed exosome-mediated drug delivery system to treat

the cancer in a precise way by dosing the therapy depending on the stage of the illness, the desired intensity of the treatment, and the genomics that affects the binding of the exosomes.

The rest of the paper is organized as follows. In Section II, we present the mathematical model of modulated exosomal release for iR-NSCs differentiated into neurons and astrocytes. As of neurons, the model is developed combining the Hodgkin-Huxley model [33] for initiation and propagation of action potentials with the Watts-Sherman- [34] and Montefusco-Pedersen model [35] for local calcium and regulated exocytosis. As of electrically silent astrocytes, the model is developed combining the Hodgkin-Huxley like formalism for inositol 1,4,5-triphosphate (IP₃) receptor-mediated oscillations of local calcium [36] with the Watts-Sherman- and Montefusco-Pedersen model. In Section III, we briefly discuss the stochastic properties of modulated exosomal release addressing the deviation from the averaged values derived in Section II. In Section IV and Section V, we present the numerical results and provide the concluding remarks, respectively.

II. MATHEMATICAL MODEL OF MODULATED EXOSOMAL RELEASE

In what follows, we opt to characterize the modulated (simplified) release of exosomes by the iR-NSCs differentiated into **neurons** and **astrocytes** [15]. Note that differentiation of iR-NSCs can also lead to a loss of the engineered properties in the therapeutic exosomes. However, in the considered scenario, we assume that the structure of the therapeutic exosomes remains intact after differentiation.

A. Modulated Exosomal Release in Neurons

In the nervous system, *synaptic exocytosis* is well-studied where calcium ions (Ca²⁺) and SNAREs (soluble N-ethylmaleimide-sensitive fusion protein attachment protein receptors) play a critical role in synaptic vesicle docking, fusion and neurotransmitter release [37]. The release is restricted to electron-dense regions called active zones which contain voltage-gated Ca²⁺ channels – P-, Q- and N-type Ca²⁺ channels – that control Ca²⁺ influx from the extracellular domain, and mediate and regulate exocytosis. Nonetheless, vesicular exocytosis has been also observed from somato-dendritic neuronal compartments [38]. For the presented study, the vesicular *somato-dendritic exocytosis* by neurons is of particular interest¹, leading to the therapeutic exosomal release in the brain extracellular matrix where, among other particles, the therapeutic exosomes propagate following the law of diffusion and ideally bind to targeted receptors in Glioblastoma cells and GSCs.

The experimental evidence reveals that exocytosis is regulated by intracellular calcium signaling in many different cell types [39], [40]. Neuron depolarization triggers electrical

activity that involves voltage-gated Ca²⁺ channels. The resulting opening of voltage-gated Ca²⁺ channels and an increase in the cytosolic calcium concentration evoke exocytosis and the release of exosomes among other secretory vesicles like synaptic-like microvesicles, lysosomes and ectosomes [25], [41], [42]. In somato-dendritic exocytosis, the release is mostly restricted to active zones that contain L-type Ca²⁺ channels [43].

We use the well-known Hodgkin-Huxley neuron model to describe the electrical activity of a depolarized neuron via membrane potential (v_m) that is dependent on voltage-gated potassium (K⁺) channels, voltage-gated sodium (Na⁺) channels, a leak current, and an induced control current (i_{ind}) as [33]:

$$\frac{dv_m}{dt} = -\frac{1}{c_m} \left[g_K (v_m - V_K) + g_{Na} (v_m - V_{Na}) + g_L (v_m - V_L) - \underbrace{i_{ind}}_{\text{control}} \right], \quad (1)$$

where c_m is specific membrane capacitance, V_K , V_{Na} and V_L are Nernst potentials for K⁺ ions, Na⁺ ions and other ions lumped together as “leak” channel, respectively, and g_K , g_{Na} and g_L are the corresponding membrane conductances. Voltage-gated conductances $g_K = \bar{g}_K m_K^4$ and $g_{Na} = \bar{g}_{Na} m_{Na}^3 h_{Na}$ change with time during an *action potential/spike* – an elementary stereotyped impulse generated and exchanged by neurons. m_K^4 and $m_{Na}^3 h_{Na}$ represent the opening probability for K⁺ and Na⁺ channels, respectively. The gating variables m_K , m_{Na} and h_{Na} and the relevant parameters are defined in Appendix A-A.

Aiming to couple neuronal electrical activity and Ca²⁺-mediated exocytosis, we first describe intracellular Ca²⁺ dynamics with particular attention to microdomain Ca²⁺ concentrations surrounding *high-voltage activated L-type Ca²⁺ channels* ([Ca]_L) and low-voltage-activated T-type Ca²⁺ channels [43], linked to a description of Ca²⁺ below the *plasma membrane* ([Ca]_m), in the *bulk cytosol* ([Ca]_c), and in the *endoplasmic reticulum* ([Ca]_{ER}). According to the evidence that somato-dendritic exocytosis by neurons shares common mechanisms with Ca²⁺-mediated exocytosis by excitable endocrine cells (where Ca²⁺ threshold of exocytosis depends on the electrical activity pattern) [44], [45], we adapt the Montefusco-Pedersen computational model initially developed for the fine-tune control of glucagon secretion in pancreatic alpha cells [35]. Glucagon secretion occurs as exocytosis of stored peptide vesicles initiated by secretory stimuli. The ultrastructural analysis indicates that the glucagon-containing vesicles have a diameter of ~ 250 nm [46], which is similar to the size of the exosome-containing endocytic compartments (~ 300 nm [16]).

Table I provides equations that describe the Ca²⁺ concentrations in single microdomains surrounding high-voltage activated L-type Ca²⁺ channels when the channels are opened and closed, sub-membrane Ca²⁺ concentration, Ca²⁺ concentration in the bulk cytosol, and Ca²⁺ concentration in the endoplasmic reticulum [35]. i_{Ca_L} and i_{Ca_T} represent the Ca²⁺ current entering the single domain through L-type Ca²⁺

¹Conversely, synaptic exocytosis leads to particle release in the extracellular matrix inside synaptic clefts. This imposes particle binding to receptors located in post-synaptic terminals, preventing released particles from reaching receptors in Glioblastoma cells and GSCs.

TABLE I
GOVERNING EQUATIONS OF MICRODOMAIN CALCIUM CONCENTRATIONS IN NEURONS

Microdomain	Equation
L-type Ca^{2+} channels	$\frac{d[\text{Ca}]_{L \text{opened}}}{dt} = -f \left(\alpha \frac{i_{\text{Ca}_L}}{\mathcal{V}_{\mu d}} - B_{\mu d} ([\text{Ca}]_L - [\text{Ca}]_m) \right); [\text{Ca}]_{L \text{closed}} \approx [\text{Ca}]_m$ (1.1)
Sub-membrane	$\frac{d[\text{Ca}]_m}{dt} = \frac{f}{\mathcal{V}_m} \left(-\alpha i_{\text{Ca}_T} + N_L \mathcal{V}_{\mu d} B_{\mu d} m_{\text{Ca}_L}^2 h_{\text{Ca}_L} ([\text{Ca}]_L - [\text{Ca}]_m) - \mathcal{V}_c k_{\text{PMCA}} [\text{Ca}]_m - \mathcal{V}_c B_m ([\text{Ca}]_m - [\text{Ca}]_c) \right)$ (1.2)
Bulk cytosol	$\frac{d[\text{Ca}]_c}{dt} = f (B_m ([\text{Ca}]_m - [\text{Ca}]_c) + p_{\text{leak}} ([\text{Ca}]_{ER} - [\text{Ca}]_c) - k_{\text{SERCA}} [\text{Ca}]_c)$ (1.3)
Endoplasmic reticulum	$\frac{d[\text{Ca}]_{ER}}{dt} = \frac{f \mathcal{V}_c}{\mathcal{V}_{ER}} (p_{\text{leak}} ([\text{Ca}]_{ER} - [\text{Ca}]_c) - k_{\text{SERCA}} [\text{Ca}]_c)$ (1.4)

channels and the sub-membrane compartment through T-type Ca^{2+} channels, respectively, and are defined as:

$$i_{\text{Ca}_L} = \frac{g_{\text{Ca}_L} (v_m - V_{\text{Ca}})}{N_L}, \quad (2)$$

$$i_{\text{Ca}_T} = g_{\text{Ca}_T} m_{\text{Ca}_T}^3 h_{\text{Ca}_T} (v_m - V_{\text{Ca}}). \quad (3)$$

where g_{Ca_L} and g_{Ca_T} are the membrane conductances of the L-type and T-type Ca^{2+} channels, respectively, $m_{\text{Ca}_L}^2 h_{\text{Ca}_L}$ and $m_{\text{Ca}_T}^3 h_{\text{Ca}_T}$ represent the opening probability for the L-type and T-type Ca^{2+} channels, respectively, V_{Ca} is the Nernst potential for Ca^{2+} ions, and N_L is the number of L-type Ca^{2+} channels. The gating variables m_{Ca_x} and h_{Ca_x} , $x \in \{T, L\}$ are defined in Appendix A-A, eqs. (32) and (33), respectively. As of the parameters used in the equations, f is the the ratio of free-to-total Ca^{2+} , α is the constant that converts current to flux, $B_{\mu d}$ is the constant that describes the flux from the microdomains to the sub-membrane, B_m is the constant that describes the flux from the sub-membrane compartment to the bulk cytosol, $\mathcal{V}_{\mu d}$, \mathcal{V}_m , \mathcal{V}_c and \mathcal{V}_{ER} are the volumes of a single microdomain, the sub-membrane compartment, the bulk cytosol, and the endoplasmic reticulum, respectively, k_{PMCA} is the rate of Ca^{2+} -ATPases through the plasma membrane, p_{leak} is the rate of the leak from endoplasmic reticulum to the cytosol, and k_{SERCA} is the rate of sarco/endoplasmic Ca^{2+} -ATPase pump-dependent sequestration of Ca^{2+} into the endoplasmic reticulum. The values of parameters given in Table I which are used to obtain the numerical results are provided in Appendix A-A, Table IV.

Following the work of Watts and Sherman for glucagon secretion in pancreatic alpha cells [34], we consider the relative exosomal release rate functions for microdomains (equivalent to the fusion rates obtained by Watts and Sherman) in neurons depending on L-type Ca^{2+} microdomain concentrations and sub-membrane Ca^{2+} concentrations, respectively, as follows:

$$\mathcal{R}_{\text{Ca}_L} = m_{\text{Ca}_L}^2 h_{\text{Ca}_L} F_H ([\text{Ca}]_{L|\text{opened}}, K_L, n_L) + (1 - m_{\text{Ca}_L}^2 h_{\text{Ca}_L}) F_H ([\text{Ca}]_{L|\text{closed}}, K_L, n_L), \quad (4)$$

$$\mathcal{R}_{\text{Ca}_m} = F_H ([\text{Ca}]_m, K_m, n_m), \quad (5)$$

where

$$F_H(x, K, n) = \phi \frac{x^n}{x^n + K^n}, \quad (6)$$

is the Hill function where ϕ is a fusion constant given in s^{-1} . K_L , n_L , K_m and n_m are given in Appendix A-A, Table IV. Note that (4) contains two terms that stem from the two states

of L-type Ca^{2+} channels, opened and closed, respectively. Considering normalized constant exosome concentrations in the considered microdomains, we define the collective exocytosis rate

$$\mathcal{R}^{(\text{neuron})}(t) = \mathcal{R}_{\text{Ca}_L}(t) + \mathcal{R}_{\text{Ca}_m}(t). \quad (7)$$

in terms of the amount of exosomes per second per liter.

Ultimately, the relative (normalized) concentration of released therapeutic neuronal exosomes depending on L-type Ca^{2+} microdomain concentrations and sub-membrane Ca^{2+} concentrations, respectively, is defined as:

$$c_{\text{Tx}}^{(\text{neuron})}(t) = c_{\text{Ca}_L}(t) + c_{\text{Ca}_m}(t), \quad (8)$$

where

$$c_{\text{Ca}_x}(t) = \int_0^t \mathcal{R}_{\text{Ca}_x}(\tau) d\tau, \quad x \in \{L, m\}. \quad (9)$$

Therefore, the whole amount of exosomes released during $[0, t]$ is given by multiplying (8) by the concentration of the exosomes around the microdomain and microdomain volume.

B. Modulated Exosomal Release in Astrocytes

Most of the existing models that describe mechanisms of astrocytic signaling that regulate release of a wide range of neurotransmitters, neuromodulators, hormones, and metabolic, trophic and plastic factors within secretory vesicles from astrocytes, also including this work, use phenomenological descriptions of gliotransmitters in which increased cytosolic Ca^{2+} concentration plays the most important role [47], [48]. The predominant sources of Ca^{2+} for exocytosis by astrocytes reside within the endoplasmic reticulum and Ca^{2+} influx through voltage-gated Ca^{2+} channels.

Similar to neurons, astrocytes have on their plasma membrane glutamate-sensitive receptors – groups I and II metabotropic glutamate receptors (mGluRs). Once activated by nearby glutamate, mGluRs trigger the intracellular release of Ca^{2+} from the endoplasmic reticulum. This process is carried out through chemical processes involving IP_3 – a secondary messenger molecule with a pivotal role in mobilizing Ca^{2+} into the cytosol. In tripartite synapses (a concept introduced to underline the presence of the astrocyte in the vicinity of two neurons), the IP_3 synthesis has been described simply under the hypothesis that a quantized amount of IP_3 molecules is released after the increase of glutamate due to pre-synaptic

spiking activity. Thus, the lifetime process of IP_3 leads to the following equation [49], [50]:

$$\frac{d[IP_3]}{dt} = \frac{[IP_{3_0}] - [IP_3]}{\tau_{IP_3}} + r_{IP_3} u(v_m - V_{th}), \quad (10)$$

where

$$\tau_{h_{IP_3}} = \frac{1}{a_2(Q + [Ca]_c)}, \quad (11)$$

$$Q = d_2 \frac{[IP_3] + d_1}{[IP_3] + d_3}. \quad (12)$$

The first term on the right side of (10) refers to the IP_3 degradation, where $[IP_{3_0}]$ is the concentration at equilibrium and τ_{IP_3} is the degradation time constant. The second term refers to the production of IP_3 , where r_{IP_3} is the production rate. The coefficients shown in (10)-(12) are given in Appendix A-B, Table V. In (10), the IP_3 production is enabled when the pre-synaptic potential v_m is above a given threshold V_{th} ($u(\cdot)$ is the Heaviside function). This is an approximation of what actually happens at the molecular level, which relates the production of IP_3 with the presence of glutamate in the synapse. In our scenario, where the astrocyte differentiated from iR-NSC acts as a neuron-independent unit, we are interested in regulating the $[IP_3]$ with a given stimulation pattern, as envisioned in Fig. 1. Thus, considering that the $[IP_3]$ production rate is a function of a generic control signal v_{ind} applied to depolarize the astrocyte, we modify (10) as

$$\frac{d[IP_3]}{dt} = \frac{[IP_{3_0}] - [IP_3]}{\tau_{IP_3}} + r_{IP_3} \underbrace{(v_{ind})}_{\text{control}}. \quad (13)$$

Of note, a practical solution to provide v_{ind} is beyond the scope of this paper and is left as future work.

We now couple (13) with Ca^{2+} dynamics to propose a model for IP_3 production and Ca^{2+} -microdomain-dependent exocytosis by electrically silent astrocytes. As with neurons, we describe Ca^{2+} dynamics with particular attention to microdomain Ca^{2+} concentrations, linked to a description of Ca^{2+} below the plasma membrane ($[Ca]_m$), in the bulk cytosol ($[Ca]_c$), and in the endoplasmic reticulum ($[Ca]_{ER}$). Electrophysiological recordings detected high-voltage activated L-type, N-type and R-type Ca^{2+} channels (in addition to low-voltage-activated T-type Ca^{2+} channels) in rat cortical astrocytes [51]. However, we describe microdomain Ca^{2+} concentrations surrounding L-type and N-type Ca^{2+} channels ($[Ca]_L$ and $[Ca]_N$), since the role of R-type Ca^{2+} channels in astrocytic exocytosis is largely unknown.

We presume the same properties of L-type Ca^{2+} channels in neurons and astrocytes [52]. Hence, Ca^{2+} concentration $[Ca]_L$ in single astrocytic microdomains is described as in neuronal microdomains (Table I) by setting $v_m = V_m + v_{ind}$ in all corresponding equations, where V_m denotes the resting astrocytic membrane potential². Table II shows equations that describe the Ca^{2+} concentrations in single microdomains surrounding high-voltage activated N-type Ca^{2+} channels when

the channels are opened and closed³, and the sub-membrane Ca^{2+} concentration [35]. i_{Ca_N} represents the Ca^{2+} current entering the single domain through N-type Ca^{2+} channels, and is defined as:

$$i_{Ca_N} = \frac{g_{Ca_N}(V_m + v_{ind} - V_{Ca})}{N_N}, \quad (14)$$

where g_{Ca_N} is the membrane conductance of the N-type Ca^{2+} channels and N_N is the number of N-type Ca^{2+} channels. $m_{Ca_N} h_{Ca_N}$ represents the opening probability for the N-type Ca^{2+} channels. The gating variables m_{Ca_N} and h_{Ca_N} are defined in Appendix A-A, eqs. (32) and (33), respectively, by replacing v_m with $V_m + v_{ind}$. Other used parameters are defined in Section II-A.

Once produced in-situ (or received from other cells through gap junction), IP_3 molecules bind to receptors located on the surface of endoplasmic reticulum enabling the release of Ca^{2+} . Since internal stores are also sensitive to Ca^{2+} , the rise of Ca^{2+} concentration mobilizes further release of Ca^{2+} . This process is called Calcium-Induced Calcium Release (CICR) [50]. Additional Ca^{2+} flow occurs spontaneously from the endoplasmic reticulum into the cytosol (leakage flow) while Ca^{2+} dependent ATPase pumps (SERCA) operate in the opposite direction to uptake Ca^{2+} back into the stores for future use (pump flow). During rest conditions, Ca^{2+} concentration is regulated by the balance between passive leakage from the endoplasmic reticulum and SERCA uptake. Ca^{2+} dynamics and the release/uptake processes triggered by IP_3 have been described analytically by Sneyd [54] and Li and Rinzel [36]. In this work, we use the Nadkarni-Jung model based on the Li-Rinzel model [55], [49], where the equations given in Table II define Ca^{2+} concentrations in the bulk cytosol and the endoplasmic reticulum. The gating variables h_{IP_3} and $m_{IP_3, \infty}$ are defined in Appendix A-B, eqs. (38) and (39), respectively. The values of used parameters in Table II are given in Appendix A-A, Table IV and Appendix A-B, Table V.

Following the work of Watts and Sherman for glucagon secretion in pancreatic alpha cells [34], we now define the relative exosomal release rate function in astrocytes depending on N-type Ca^{2+} microdomain concentrations:

$$\mathcal{R}_{Ca_N} = m_{Ca_N} h_{Ca_N} F_H([Ca]_{N|opened}, K_N, n_N) + (1 - m_{Ca_N} h_{Ca_N}) F_H([Ca]_{N|closed}, K_N, n_N). \quad (15)$$

F_H is defined in (6). K_N and n_N are given in Appendix A-B, Table V. The relative exosomal release rate functions depending on L-type Ca^{2+} microdomain concentrations and sub-membrane Ca^{2+} concentrations, \mathcal{R}_{Ca_L} and \mathcal{R}_{Ca_m} , follow (4) and (5), respectively. Considering normalized constant exosome concentrations in the considered microdomains, we define the collective exocytosis rate

$$\mathcal{R}^{(\text{astro})}(t) = \mathcal{R}_{Ca_L}(t) + \mathcal{R}_{Ca_N}(t) + \mathcal{R}_{Ca_m}(t). \quad (16)$$

³Note that Montefusco and Pedersen [35] use similar expressions for the P/Q-type Ca^{2+} channels used by Watts and Sherman [34] for the N-type Ca^{2+} channels.

²The resting membrane potentials in astrocyte range from -25 to -85 mV [53]. Here, we select $V_m = -70$ mV.

TABLE II
GOVERNING EQUATIONS OF MICRODOMAIN CALCIUM CONCENTRATIONS IN ASTROCYTES

Microdomain	Equation	
N-type Ca ²⁺ channels	$\frac{d[\text{Ca}]_{N \text{opened}}}{dt} = -f \left(\alpha \frac{i_{\text{Ca}_N}}{\mathcal{V}_{\mu d}} - B_{\mu d} ([\text{Ca}]_N - [\text{Ca}]_m) \right); [\text{Ca}]_{N \text{closed}} \approx [\text{Ca}]_m$	(II.1)
Sub-membrane	$\frac{d[\text{Ca}]_m}{dt} = \frac{f}{\mathcal{V}_m} \left(-\alpha i_{\text{Ca}_T} + N_L \mathcal{V}_{\mu d} B_{\mu d} m_{\text{Ca}_L}^2 h_{\text{Ca}_L} ([\text{Ca}]_L - [\text{Ca}]_m) + N_N \mathcal{V}_{\mu d} B_{\mu d} m_{\text{Ca}_N} h_{\text{Ca}_N} ([\text{Ca}]_N - [\text{Ca}]_m) - \mathcal{V}_c k_{\text{PMCA}} [\text{Ca}]_m - \mathcal{V}_c B_m ([\text{Ca}]_m - [\text{Ca}]_c) \right)$	(II.2)
Bulk cytosol	$\frac{d[\text{Ca}]_c}{dt} = - \underbrace{c_1 v_1 m_{\text{IP}_3, \infty}^3 h_{\text{IP}_3}^3 ([\text{Ca}]_c - [\text{Ca}]_{ER})}_{\text{CICR}} - \underbrace{c_1 v_2 ([\text{Ca}]_c - [\text{Ca}]_{ER})}_{\text{leak}} - \underbrace{v_3 \frac{[\text{Ca}]_c^2}{k_3^2 + [\text{Ca}]_c^2}}_{\text{uptake}}$	(II.3)
Endoplasmic reticulum	$[\text{Ca}]_{ER} = \frac{c_0 - [\text{Ca}]_c}{c_1}$	(II.4)

Ultimately, the relative (normalized) concentration of released therapeutic astrocytic exosomes depending on L-type and N-type Ca²⁺ microdomain concentrations and sub-membrane Ca²⁺ concentrations, respectively, is defined as:

$$c_{\text{Tx}}^{(\text{astro})}(t) = c_{\text{Ca}_L}(t) + c_{\text{Ca}_N}(t) + c_{\text{Ca}_m}(t), \quad (17)$$

where

$$c_{\text{Ca}_x}(t) = \int_0^t \mathcal{R}_{\text{Ca}_x}(\tau) d\tau, \quad x \in \{L, N, m\}. \quad (18)$$

III. STOCHASTIC PROPERTIES OF MODULATED EXOSOMAL RELEASE

In the previous section, we implicitly assumed that the release events of the exosomes from different domains of the membrane were statistically independent. This assumption is justified by considering the following:

- We assume that the cells can regenerate and replenish the exosomes whenever the exosomes are released. This is a more reasonable and realistic assumption for neurons in which the refractory period between the spikes enables the time to replenish the storage of the exosomes, in addition to the re-polarization process.
- We assume that the exosomes are distributed through different domains of the cell membrane whose release permeabilities are modulated through independent ion channels in different microdomains.

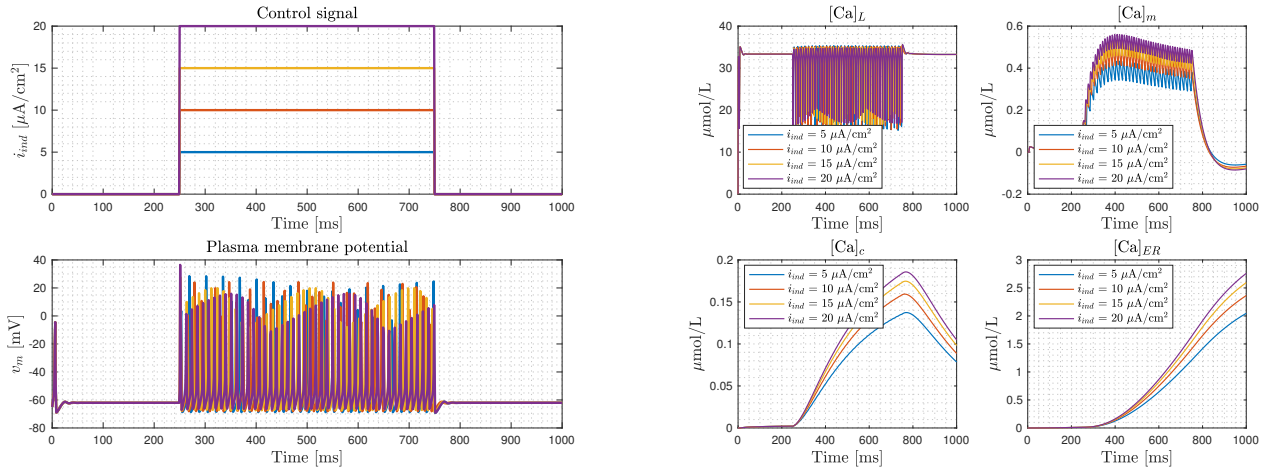
Nonetheless, due to the many stochastic phenomena, the modulated exosomal release deviates from the average values evaluated in the previous section. We thus model the exosomal release process as a Poisson process whose rate is $\mathcal{R}_v(t) = \mathcal{R}^{(\text{cell})}(t)/\mathbb{E}[N_e]$, in which $\mathcal{R}^{(\text{cell})}(t)$ is the exosomal release rate for neurons or astrocytes proportional to the rates in (7) and (16), respectively, and $\mathbb{E}[N_e]$ is the average number of the exosomes contained in a fused intermediate endocytic compartment (multivesicular body). The total number of the released exosomes (\mathcal{N}) can thus be estimated as a compound Poisson process $\mathcal{N} = \sum_{i=1}^{N_v(t)} N_e^i$, in which $N_v(t)$ is the total number of release events that follows the inhomogeneous Poisson process with the rate $\mathcal{R}_v(t)$, and N_e^i s are the independent identically distributed random variables that represent the number of exosomes in the i^{th} release event.

IV. NUMERICAL RESULTS

The numerical results provided in this section are obtained using the parameter values collected from [33] and [49], and from [35] (for pancreatic cells). Some of the presented results are thus unrealistic (e.g., the negative Ca²⁺ concentrations for astrocytic microdomains), but are presented to primarily illustrate the application of the proposed methodology. The simulation framework has been implemented in MATLAB.

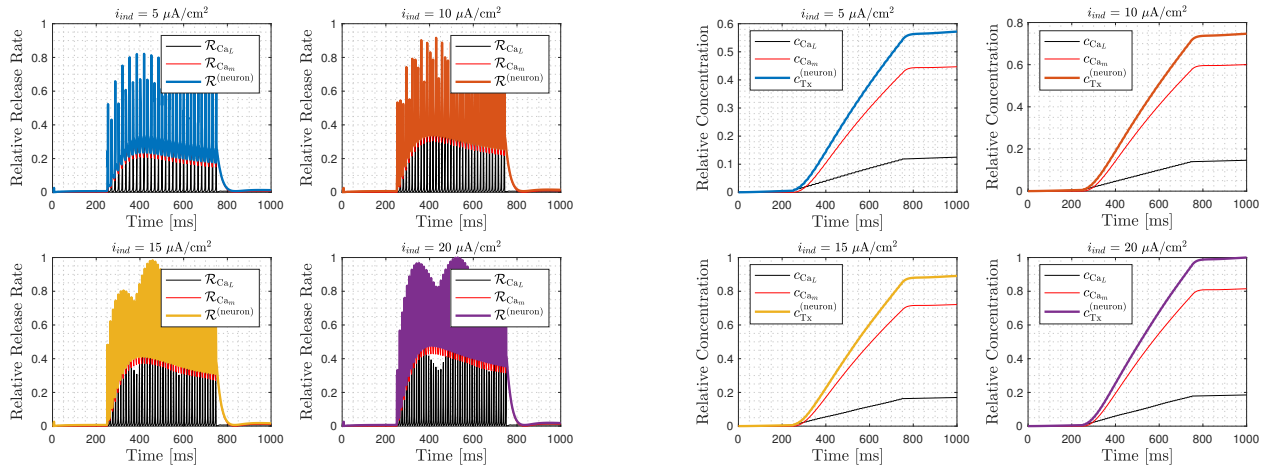
The effects of the controlled exocytosis by neurons differentiated from iR-NSCs are depicted in Fig. 3 using the induced current pulses of 500 ms duration and amplitudes ranging from 5–20 $\mu\text{A}/\text{cm}^2$ (Fig. 3(a), upper plot). Neurons are electrically excitable and respond to the provided stimuli by creating sequences of action potentials with the rate proportional to the stimuli (Fig. 3(a), lower plot). The spiking sequences further control the dynamics of voltage-gated calcium channels in the membrane, which, in turn, control the intracellular Ca²⁺ concentration near open or closed Ca²⁺ channels (of L-type), below the plasma membrane, in the bulk cytosol and the endoplasmic reticulum. The concentrations are evaluated by equations provided in Table I and shown in Fig. 3(b). The rates of released exosomes with relative contributions of the Ca²⁺ compartments are evaluated by (4), (5) and (7) and shown in Fig. 3(c) where we observe action-potential driven oscillations around the baseline values that increase with the stimuli intensity. When the stimulation is interrupted at $t = 750$ ms, the release fades after ~ 50 ms. The corresponding concentrations of released exosomes are evaluated by (8) and (9). Under the assumption of having non-depleted readily releasable exosomes in the cytosol throughout the stimulation period, we observe an approximately linear increase in the concentration of released exosomes for all stimuli intensities. We also observe that for the considered scenario, $\sim 70\%$ of the concentration of released exosomes stems from the concentration dependent on sub-membrane Ca²⁺ concentrations.

As of astrocytes, the $[\text{IP}_3]$ production rate function $r_{\text{IP}_3}(v_{\text{ind}})$ given in (13) has not been characterized in the literature to the best of our knowledge. Therefore, to obtain the numerical results, we simply assume that $[\text{IP}_3]$ production is linearly proportional to the intensity of depolarization v_{ind} . The effects of the controlled exocytosis by astrocytes differentiated from iR-NSCs are depicted in Fig. 4 using the



(a) Induced control signals/currents and the corresponding responses/spiking sequences in the depolarized neuron.

(b) Microdomain calcium concentrations corresponding to the control signals shown in Fig. 3(a).



(c) The exocytosis rate functions corresponding to the control signals shown in Fig. 3(a). The values are normalized using the maximum values from the fourth scenario.

(d) The concentrations of released exosomes corresponding to the control signals shown in Fig. 3(a). The values are normalized using the maximum values from the fourth scenario.

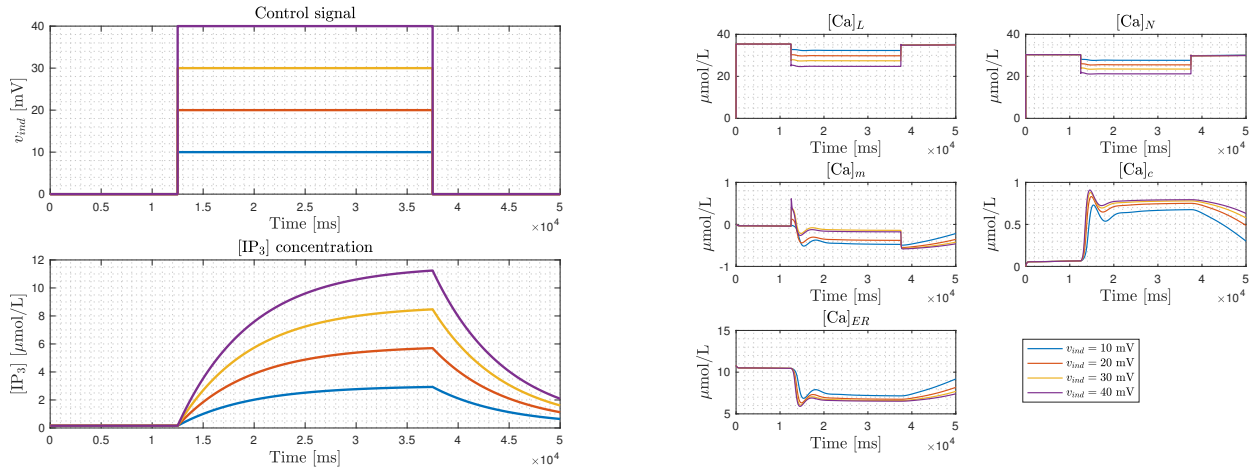
Fig. 3. Modulated exocytosis by neurons differentiated from iR-NSCs. The quantities are evaluated using the parameter sets given in Table III and Table IV, Appendix A-A.

generic control signals of 25.0 s duration and amplitudes ranging from 10 – 40 mV (Fig. 4(a), upper plot). Astrocytes respond to depolarization by triggering the production of IP_3 molecules whose concentration is an exponential function of the membrane potential intensity (Fig. 4(a), lower plot). IP_3 mobilizes Ca^{2+} into the cytosol. The Ca^{2+} concentrations near open or closed Ca^{2+} channels (of L- and N-type), below the plasma membrane, in the bulk cytosol and the endoplasmic reticulum are evaluated by equations provided in Table II and shown in Fig. 4(b). The corresponding rates of released exosomes with relative contributions of the Ca^{2+} compartments are evaluated by (4), (15) and (16) and shown in Fig. 4(c) where one can approximate them as constant during the controlling phase. When the control signal is interrupted at $t = 37.5$ s, the release slows down to zero. The corresponding concentrations of released exosomes are evaluated by (17) and (18). Under the assumption of having non-depleted readily releasable exosomes in the cytosol, we observe the increase

in the concentration of released exosomes for all tested stimuli intensities. We also observe that for the considered parameter set, the total concentration of released exosomes mostly stems from the concentration dependent on N-type Ca^{2+} concentrations and sub-membrane Ca^{2+} concentrations for weak depolarization (the first two scenarios), and the concentration dependent on N-type Ca^{2+} concentrations for strong depolarization (the third and fourth scenario).

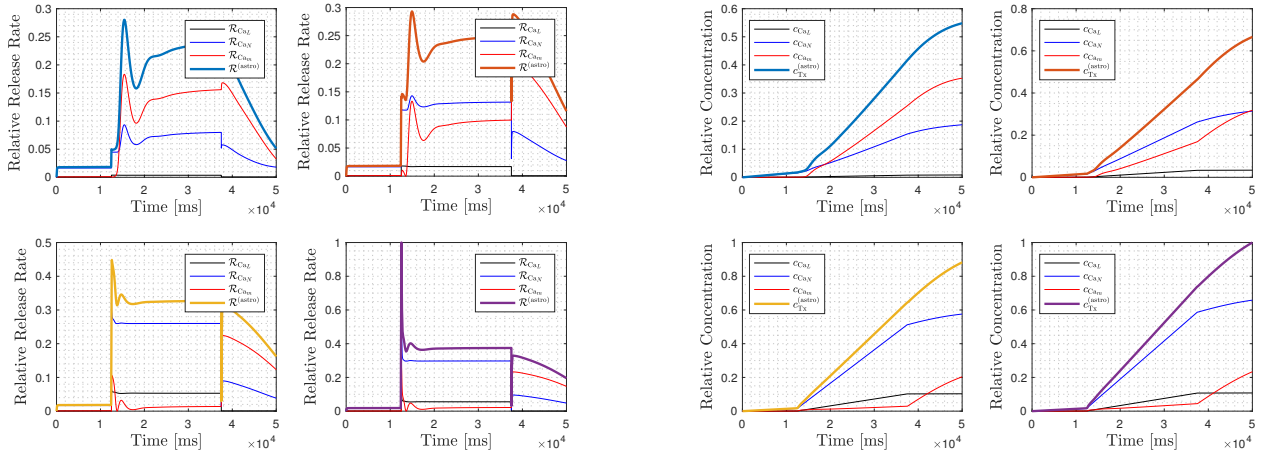
Unlike neurons, astrocytes are electrically silent and unable to generate action potentials. This implies different mechanisms that trigger the elevation of astrocyte intracellular Ca^{2+} levels, including chemical processes involving IP_3 . These mechanisms have significantly slower dynamics compared to neural spiking, thus imposing the significantly slower dynamics of exocytosis by astrocytes compared to exocytosis by neurons, as shown in Fig. 3 and Fig. 4.

Finally, as of the *cellular performance*, higher release rate and exosome concentrations from neurons and astrocytes mean



(a) Generic control signals and the corresponding IP_3 concentrations in the astrocyte.

(b) Microdomain calcium concentrations corresponding to the control signals shown in Fig. 4(a).



(c) The exocytosis rate functions corresponding to the control signals shown in Fig. 4(a). The values are normalized using the maximum values from the fourth scenario.

(d) The concentrations of released exosomes corresponding to the control signals shown in Fig. 4(a). The values are normalized using the maximum values from the fourth scenario.

Fig. 4. Modulated exocytosis by astrocytes differentiated from iR-NSCs. The quantities are evaluated using the parameter set given in Table V, Appendix A-B.

better response to depolarization. Although neurons and astrocyte both react positively in that context, the later demonstrate a more prominent increase in release rates in response to the applied signals. As of the *drug delivery performance*, however, higher release rates and exosome concentrations do not necessarily mean better therapy. This rather depends on each individual and clinical setup.

V. CONCLUSION

The overarching goal of our research is to deliver a multi-functional and multi-modal brain tumor reprogramming and monitoring platform based on autonomous, externally controllable molecular communication technology for the management of malignant brain tumors. The platform will integrate hybrid (electronic + biological) nanosensors, multi-functional autologous organoids and enabling brain molecule-machine interfaces. Autologous organoids consist of engineered iNSCs to synthesize and release rationally designed therapeutic exo-

somes. The iNSCs are envisioned to be equipped by promoters sensitive to specific wavelengths in the electromagnetic spectrum, which enables the modulation of exosomal release by providing stimulation patterns via in-messaging interfaces. Thereby, it is required to model the exosomal release from the iNSCs to study the feasibility and potential of the envisioned system. Moreover, new models could be used in designing and optimizing the target platform.

In this paper, we proposed an integrated mathematical model for the therapeutic exosomal release modulated by the stimulus externally applied to the neurons and astrocytes differentiated from iNSCs within safety guidelines. The proposed models integrate cell stimulation, intercellular signaling, and exocytosis, and provide insights into the relative contributions of the various subcellular Ca^{2+} compartments in the control of exosomal release. According to the results presented in Fig. 3 and Fig. 4, we infer the positive effect of cell depolarization in both neurons and astrocytes on the exosomal release,

TABLE III
PARAMETER SET (ELECTRICAL ACTIVITY OF NEURONS) [33]

Parameter	Nominal value	Unit
g_K	36	mS/cm ³
V_K	-70	mV
\bar{g}_{Na}	120	mS/cm ³
V_{Na}	50	mV
g_L	0.3	mS/cm ³
V_L	-54.4	mV
c_m	1	μF/cm ²

where the intensity of the exosomal release is proportional to the intensity of applied stimulation. We considered noiseless stimulation which is very unlikely to occur in-vivo. The set of control interfering noise sources will depend on the future selected technology to deliver depolarizing signals to therapeutic bio-nanomachines for the envisioned treatment of Glioblastoma. A number of technologies have been developed to target specific cell types for stimulation, such as optogenetics, where the cells are engineered to respond to light at a specific wavelength. Therefore, through this technique, minimization of noise can be achieved when only selected cells are targeted for stimulation.

Based on the models, we will develop the controlled transmission of exosomes in the brain in a closed-loop manner and provide an avenue for developing new tools that can be used to deliver drugs and treat cancerous cells leading to advanced engineering technologies. We will further use the computed exosomal release rates as input to the end-to-end communication model that we plan to develop in the next step. The information capacity will be used to evaluate the system performance and as an objective function encompassing all relevant system parameters to optimize its design. In this way, we believe that optimized drug delivery systems based on exosomes would redefine the current medical treatment strategies.

VI. ACKNOWLEDGEMENT

This work was supported in part by the EU under grants #828837 (EU-H2020-FETOpen GLADIATOR Next-generation Theranostics of Brain Pathologies with Autonomous Externally Controllable Nanonetworks: a Transdisciplinary Approach with Bio-nanodevice Interfaces), and the Research Council of Norway under grant #270957 (RCN:WINNOW Wireless In-body Sensor and Actuator Networks).

APPENDIX A

SUPPLEMENTARY EQUATIONS AND PARAMETERS OF THE MODEL

A. Neurons

Gating variables (m_K , m_{Na} and h_{Na}):

$$\frac{dm_{K/Na}}{dt} = \frac{m_{K/Na,\infty}(v_m) - m_{K/Na}}{\tau_{m_{K/Na}}(v_m)} \quad (19)$$

$$\frac{dh_{Na}}{dt} = \frac{h_{Na,\infty}(v_m) - h_{Na}}{\tau_{h_{Na}}(v_m)} \quad (20)$$

TABLE IV
PARAMETER SET (CALCIUM DYNAMICS AND EXOCYTOSIS BY NEURONS) [35]

Parameter	Nominal value	Unit
g_{CaL}	0.7	nS
g_{CaT}	0.4	nS
V_{Ca}	65	mV
$V_{m_{CaL}}$	-30	mV
$S_{m_{CaL}}$	10	mV
$V_{h_{CaL}}$	-33	mV
$S_{h_{CaL}}$	-5	mV
$\tau_{m_{V_{CaL}}}$	1	ms
$\tau_{m0_{V_{CaL}}}$	0.05	ms
$V_{\tau_{m_{CaL}}}$	-23	mV
$S_{\tau_{m_{CaL}}}$	20	mV
$\tau_{h_{V_{CaL}}}$	60	ms
$\tau_{h0_{V_{CaL}}}$	51	ms
$V_{\tau_{h_{CaL}}}$	0	mV
$S_{\tau_{h_{CaL}}}$	20	mV
$V_{m_{CaT}}$	-49	mV
$S_{m_{CaT}}$	4	mV
$V_{h_{CaT}}$	-52	mV
$S_{h_{CaT}}$	-5	mV
$\tau_{m_{V_{CaT}}}$	15	ms
$\tau_{m0_{V_{CaT}}}$	0	ms
$V_{\tau_{m_{CaT}}}$	-50	mV
$S_{\tau_{m_{CaT}}}$	12	mV
$\tau_{h_{V_{CaT}}}$	20	ms
$\tau_{h0_{V_{CaT}}}$	5	ms
$V_{\tau_{h_{CaT}}}$	-50	mV
$S_{\tau_{h_{CaT}}}$	15	mV
f	0.01	-
α	5.180×10^{-15}	μmol pA ⁻¹ ms ⁻¹
$V_{\mu d}$	2.618×10^{-19}	L
V_m	5.149×10^{-14}	L
V_c	5.725×10^{-13}	L
V_c/V_{ER}	31	-
$B_{\mu d}$	264	ms ⁻¹
B_m	0.128	ms ⁻¹
k_{PMCA}	0.300	ms ⁻¹
k_{SERCA}	0.100	ms ⁻¹
p_{leak}	3×10^{-4}	ms ⁻¹
N_L	200	-
n_L	4	-
K_L	50	μM
n_m	4	-
K_m	2	μM

Gating variables in the steady state:

$$m_{K/Na,\infty} = \frac{\alpha_{m_{K/Na}}}{\alpha_{m_{K/Na}} + \beta_{m_{K/Na}}} \quad (21)$$

$$h_{Na,\infty} = \frac{\alpha_{h_{Na}}}{\alpha_{h_{Na}} + \beta_{h_{Na}}} \quad (22)$$

Time constants and gating functions:

$$\tau_{m_{K/Na}} = \frac{1}{\alpha_{m_{K/Na}} + \beta_{m_{K/Na}}} \quad (23)$$

$$\tau_{h_{Na}} = \frac{1}{\alpha_{h_{Na}} + \beta_{h_{Na}}} \quad (24)$$

$$\alpha_{m_K} = \frac{0.01(v_m + 55)}{1 - F_E(v_m, 55, 10)} \quad (25)$$

$$\beta_{m_K} = 0.125 F_E(v_m, 65, 80) \quad (26)$$

$$\alpha_{m_{Na}} = \frac{0.1(v_m + 40)}{1 - F_E(v_m, 40, 10)} \quad (27)$$

$$\beta_{m_{Na}} = 4 F_E(v_m, 65, 18) \quad (28)$$

$$\alpha_{h_{Na}} = 0.07 F_E(v_m, 65, 20) \quad (29)$$

$$\beta_{h_{Na}} = \frac{1}{1 + F_E(v_m, 35, 10)} \quad (30)$$

where

$$F_E(v, a, b) = \exp\left(\frac{-(v+a)}{b}\right) \quad (31)$$

Gating variables ($x \in \{T, L, N\}$):

$$\frac{dm_{Ca_x}}{dt} = \frac{m_{Ca_x, \infty}(v_m) - m_{Ca_x}}{\tau_{m_{Ca_x}}(v_m)} \quad (32)$$

$$\frac{dh_{Ca_x}}{dt} = \frac{h_{Ca_x, \infty}(v_m) - h_{Ca_x}}{\tau_{h_{Ca_x}}(v_m)} \quad (33)$$

Gating variables in the steady state:

$$m_{Ca_x, \infty} = \frac{1}{1 + \exp\left(-\frac{v_m - V_{m_{Ca_x}}}{S_{m_{Ca_x}}}\right)} \quad (34)$$

$$h_{Ca_x, \infty} = \frac{1}{1 + \exp\left(-\frac{v_m - V_{h_{Ca_x}}}{S_{h_{Ca_x}}}\right)} \quad (35)$$

Time constants:

$$\tau_{m_{Ca_x}} = \frac{\tau_{m_{V_{Ca_x}}}}{\exp\left(-\frac{v_m - V_{\tau_{m_{Ca_x}}}}{S_{\tau_{m_{Ca_x}}}}\right) + \exp\left(\frac{v_m - V_{\tau_{m_{Ca_x}}}}{S_{\tau_{m_{Ca_x}}}}\right)} + \tau_{m_{0V_{Ca_x}}} \quad (36)$$

$$\tau_{h_{Ca_x}} = \frac{\tau_{h_{V_{Ca_x}}}}{\exp\left(-\frac{v_m - V_{\tau_{h_{Ca_x}}}}{S_{\tau_{h_{Ca_x}}}}\right) + \exp\left(\frac{v_m - V_{\tau_{h_{Ca_x}}}}{S_{\tau_{h_{Ca_x}}}}\right)} + \tau_{h_{0V_{Ca_x}}} \quad (37)$$

The parameters shown in (34)-(37) are given in Table IV.

B. Astrocytes

Gating variable (h_{IP_3}):

$$\frac{dh_{IP_3}}{dt} = \frac{h_{IP_3, \infty} - h_{IP_3}}{\tau_{h_{IP_3}}} \quad (38)$$

Gating variables in the steady state ($m_{IP_3, \infty}$ and $h_{IP_3, \infty}$):

$$m_{IP_3, \infty} = \left(\frac{[IP_3]}{[IP_3] + d_1}\right) \left(\frac{[Ca]_c}{[Ca]_c + d_5}\right) \quad (39)$$

$$h_{IP_3, \infty} = \frac{Q}{Q + [Ca]_c} \quad (40)$$

The parameter shown in (38) and (39) are given in Table V.

TABLE V
PARAMETER SET (IP₃- AND CALCIUM DYNAMICS AND EXOCYTOSIS BY ASTROCYTES) [35], [49]

Parameter	Nominal value	Unit
c_0	2	μM
c_1	0.185	-
v_1	6	s^{-1}
v_2	0.11	s^{-1}
v_3	0.9	$\mu\text{M/s}$
k_3	0.1	μM
d_1	0.13	-
d_2	1.049	-
d_3	0.943	-
d_5	0.082	-
a_2	0.5	$1/(\mu\text{M s})$
IP_{30}	0.160	μM
r_{IP_3}	0.04	$\mu\text{M/s}$
τ_{IP_3}	1/0.000140	ms
V_m	-70	mV
g_{Ca_N}	0.6	nS
$V_{m_{Ca_N}}$	-5	mV
$S_{m_{Ca_N}}$	10	mV
$V_{h_{Ca_N}}$	-33	mV
$S_{h_{Ca_N}}$	-5	mV
$\tau_{m_{V_{Ca_N}}}$	1	ms
$\tau_{m_{0V_{Ca_N}}}$	0.05	ms
$V_{\tau_{m_{Ca_N}}}$	-23	mV
$S_{\tau_{m_{Ca_N}}}$	20	mV
$\tau_{h_{V_{Ca_N}}}$	60	ms
$\tau_{h_{0V_{Ca_N}}}$	51	ms
$V_{\tau_{h_{Ca_N}}}$	0	mV
$S_{\tau_{h_{Ca_N}}}$	20	mV
N_N	200	-
n_N	4	-
K_N	2	μM

REFERENCES

- [1] X. Dong, "Current strategies for brain drug delivery," *Theranostics*, vol. 8, no. 6, pp. 1481–1493, 2018.
- [2] I. Mäger, A. H. Meyer, J. Li, M. Lenter, T. Hildebrandt, G. Leparic, and M. J. A. Wood, "Targeting blood-brain-barrier transcytosis - perspectives for drug delivery," *Neuropharmacology*, vol. 120, pp. 4–7, 2017.
- [3] Y. Chahibi, M. Pierobon, S. O. Song, and I. F. Akyildiz, "A molecular communication system model for particulate drug delivery systems," *IEEE Transactions on Biomedical Engineering*, vol. 60, no. 12, pp. 3468–3483, 2013.
- [4] Y. Chahibi, M. Pierobon, and I. F. Akyildiz, "Pharmacokinetic modeling and biodistribution estimation through the molecular communication paradigm," *IEEE Transactions on Biomedical Engineering*, vol. 62, no. 10, pp. 2410–2420, 2015.
- [5] M. Femminella, G. Reali, and A. V. Vasilakos, "A molecular communications model for drug delivery," *IEEE Transactions on NanoBioscience*, vol. 14, no. 8, pp. 935–945, 2015.
- [6] U. A. K. Chude-Onkonkwo, R. Malekian, B. T. Maharaj, and A. V. Vasilakos, "Molecular communication and nanonetwork for targeted drug delivery: A survey," *IEEE Communications Surveys Tutorials*, vol. 19, no. 4, pp. 3046–3096, 2017.
- [7] T. Nakano, S. Kobayashi, T. Suda, Y. Okaie, Y. Hiraoka, and T. Haraguchi, "Externally controllable molecular communication," *IEEE Journal on Selected Areas in Communications*, vol. 32, no. 12, pp. 2417–2431, 2014.
- [8] M. Veletić, M. T. Barros, I. Balasingham, and S. Balasubramaniam, "A molecular communication model of exosome-mediated brain drug delivery," in *Proceedings of the Sixth Annual ACM International Conference on Nanoscale Computing and Communication*, pp. 22:1–7, 2019.
- [9] E. J. Bunggulawa, W. Wang, T. Yin, N. Wang, C. Durkan, Y. Wang, and G. Wang, "Recent advancements in the use of exosomes as drug delivery systems," *Journal of Nanobiotechnology*, vol. 16:81, no. 1, pp. 1–13, 2018.

- [10] J. E. Pullan, M. I. Confeld, J. K. Osborn, J. Kim, K. Sarkar, and S. Mallik, "Exosomes as drug carriers for cancer therapy," *Molecular Pharmaceutics*, vol. 16, pp. 1789–1798, 05 2019.
- [11] Z. Yang, J. Shi, J. Xie, Y. Wang, J. Sun, T. Liu, Y. Zhao, X. Zhao, X. Wang, Y. Ma, V. Malkoc, C. Chiang, W. Deng, Y. Chen, Y. Fu, K. J. Kwak, Y. Fan, C. Kang, C. Yin, J. Rhee, P. Bertani, J. Otero, W. Lu, K. Yun, A. S. Lee, W. Jiang, L. Teng, B. Y. S. Kim, and L. J. Lee, "Large-scale generation of functional mRNA-encapsulating exosomes via cellular nanoporation," *Nature Biomedical Engineering*, vol. 4, no. 1, pp. 69–83, 2020.
- [12] M. Piffoux, A. K. A. Silva, C. Wilhelm, F. Gazeau, and D. Tareste, "Modification of extracellular vesicles by fusion with liposomes for the design of personalized biogenic drug delivery systems," *ACS Nano*, vol. 12, no. 7, pp. 6830–6842, 2018.
- [13] C. Altaner and U. Altanerova, "Mesenchymal stem cell exosome-mediated prodrug gene therapy for cancer," in *Suicide Gene Therapy*, pp. 75–85, Springer, 2019.
- [14] M. Ruggieri, G. Riboldi, S. Brajkovic, M. Bucchia, N. Bresolin, G. P. Comi, and S. Corti, "Induced neural stem cells: Methods of reprogramming and potential therapeutic applications," *Progress in Neurobiology*, vol. 114, pp. 15–24, 2014.
- [15] K. Hemmer, M. Zhang, T. van Wüllen, M. Sakalem, N. Tapia, A. Baumuratov, C. Kaltschmidt, B. Kaltschmidt, H. R. Schöler, W. Zhang, and J. C. Schwamborn, "Induced neural stem cells achieve long-term survival and functional integration in the adult mouse brain," *Stem Cell Reports*, vol. 3, no. 3, pp. 423–431, 2014.
- [16] J. R. Edgar, "Q&A: What are exosomes, exactly?," *BMC biology*, vol. 14:46, pp. 1–7, 2016.
- [17] P. Sharma, P. Mesci, C. Carroumeu, D. R. McClatchy, L. Schiapparelli, J. R. Yates, A. R. Muotri, and H. T. Cline, "Exosomes regulate neurogenesis and circuit assembly," *Proceedings of the National Academy of Sciences*, vol. 116, no. 32, pp. 16086–16094, 2019.
- [18] C. Fröhlich, D. Fröhlich, and E.-M. Kramer-Albers, "Emerging roles of exosomes in neuroglia communication," *Frontiers in Physiology*, vol. 3, pp. 119:1–7, 2012.
- [19] A. M. Janas, K. Sapo, T. Janas, M. H. Stowell, and T. Janas, "Exosomes and other extracellular vesicles in neural cells and neurodegenerative diseases," *Biochimica et Biophysica Acta (BBA) - Biomembranes*, vol. 1858, no. 6, pp. 1139–1151, 2016.
- [20] Y. Men, J. Yelick, S. Jin, Y. Tian, M. S. R. Chiang, H. Higashimori, E. Brown, R. Jarvis, and Y. Yang, "Exosome reporter mice reveal the involvement of exosomes in mediating neuron to astroglia communication in the CNS," *Nature Communications*, vol. 10, no. 1, pp. 4136:1–18, 2019.
- [21] S. K. Gruzdev, A. A. Yakovlev, T. A. Druzhkova, A. B. Guekht, and N. V. Gulyaeva, "The missing link: How exosomes and mirnas can help in bridging psychiatry and molecular biology in the context of depression, bipolar disorder and schizophrenia," *Cellular and Molecular Neurobiology*, vol. 39, no. 6, pp. 729–750, 2019.
- [22] S. Saeedi, S. Israel, C. Nagy, and G. Turecki, "The emerging role of exosomes in mental disorders," *Translational Psychiatry*, vol. 9, no. 1, pp. 122:1–11, 2019.
- [23] A. Venturini, M. Passalacqua, S. Pelassa, F. Pastorino, M. Tedesco, K. Cortese, M. C. Gagliani, G. Leo, G. Maura, D. Guidolin, L. F. Agnati, M. Marcoli, and C. Cervetto, "Exosomes from astrocyte processes: Signaling to neurons," *Frontiers in pharmacology*, vol. 10, pp. 1452–1452, 12 2019.
- [24] B. Ataman, J. Ashley, M. Gorczyca, P. Ramachandran, W. Fouquet, S. J. Sigrist, and V. Budnik, "Rapid activity-dependent modifications in synaptic structure and function require bidirectional Wnt signaling," *Neuron*, vol. 57, no. 5, pp. 705–718, 2008.
- [25] G. Lachenal, K. Pernet-Gallay, M. Chivet, F. J. Hemming, A. Belly, G. Bodon, B. Blot, G. Haase, Y. Goldberg, and R. Sadoul, "Release of exosomes from differentiated neurons and its regulation by synaptic glutamatergic activity," *Molecular and Cellular Neuroscience*, vol. 46, no. 2, pp. 409–418, 2011.
- [26] J. K. Jaiswal, M. Fix, T. Takano, M. Nedergaard, and S. M. Simon, "Resolving vesicle fusion from lysis to monitor calcium-triggered lysosomal exocytosis in astrocytes," *Proceedings of the National Academy of Sciences*, vol. 104, no. 35, pp. 14151–14156, 2007.
- [27] T. Liu, L. Sun, Y. Xiong, S. Shang, N. Guo, S. Teng, Y. Wang, B. Liu, C. Wang, L. Wang, L. Zheng, C. X. Zhang, W. Han, and Z. Zhou, "Calcium triggers exocytosis from two types of organelles in a single astrocyte," *Journal of Neuroscience*, vol. 31, no. 29, pp. 10593–10601, 2011.
- [28] H. Zhou, L. Niu, L. Meng, Z. Lin, J. Zou, X. Xia, X. Huang, W. Zhou, T. Bian, and H. Zheng, "Noninvasive ultrasound deep brain stimulation for the treatment of Parkinson's disease model mouse," *Research (Washington, D.C.)*, vol. 2019, pp. 1–13, 2019.
- [29] N. Feliu, E. Neher, and W. J. Parak, "Toward an optically controlled brain," *Science*, vol. 359, no. 6376, pp. 633–634, 2018.
- [30] S. Balasubramaniam, S. A. Wirdatmadja, M. T. Barros, Y. Koucheryavy, M. Stachowiak, and J. M. Jorner, "Wireless communications for optogenetics-based brain stimulation: Present technology and future challenges," *IEEE Communications Magazine*, vol. 56, no. 7, pp. 218–224, 2018.
- [31] M. Lu, B. Huang, S. M. Hanash, J. Onuchic, and E. Ben-Jacob, "Modeling putative therapeutic implications of exosome exchange between tumor and immune cells," *Proceedings of the National Academy of Sciences of the United States of America*, vol. 111, pp. E4165–E4174, 10 2014.
- [32] A. Friedman and W. Hao, "The role of exosomes in pancreatic cancer microenvironment," *Bulletin of Mathematical Biology*, vol. 80, no. 5, pp. 1111–1133, 2018.
- [33] A. L. Hodgkin and A. F. Huxley, "A quantitative description of membrane current and its application to conduction and excitation in nerve," *The Journal of physiology*, vol. 117, no. 4, pp. 500–544, 1952.
- [34] M. Watts and A. Sherman, "Modeling the pancreatic α -cell: dual mechanisms of glucose suppression of glucagon secretion," *Biophysical Journal*, vol. 106, no. 3, pp. 741–751, 2014.
- [35] F. Montefusco and M. G. Pedersen, "Mathematical modelling of local calcium and regulated exocytosis during inhibition and stimulation of glucagon secretion from pancreatic alpha-cells," *The Journal of physiology*, vol. 593, no. 20, pp. 4519–4530, 2015.
- [36] Y.-X. Li and J. Rinzel, "Equations for InsP3 receptor-mediated $[Ca^{2+}]_i$ oscillations derived from a detailed kinetic model: A Hodgkin-Huxley like formalism," *Journal of Theoretical Biology*, vol. 166, no. 4, pp. 461–473, 1994.
- [37] T. C. Südhof and J. Rizo, "Synaptic vesicle exocytosis," *Cold Spring Harbor perspectives in biology*, vol. 3, no. 12, pp. 1–14, 2011.
- [38] C. Fröhlich, D. Fröhlich, W. P. Kuo, and E.-M. Krämer-Albers, "Extracellular vesicles as mediators of neuron-glia communication," *Frontiers in cellular neuroscience*, vol. 7, pp. 182–182, 2013.
- [39] J. T. Low, A. Shukla, N. Behrendorff, and P. Thorn, "Exocytosis, dependent on Ca^{2+} release from Ca^{2+} stores, is regulated by Ca^{2+} microdomains," *Journal of Cell Science*, vol. 123, no. 18, pp. 3201–3208, 2010.
- [40] M. G. Pedersen, A. Tagliavini, G. Cortese, M. Riz, and F. Montefusco, "Recent advances in mathematical modeling and statistical analysis of exocytosis in endocrine cells," *Mathematical Biosciences*, vol. 283, pp. 60–70, 2017.
- [41] C. Trueta and F. F. De-Miguel, "Extrasynaptic exocytosis and its mechanisms: a source of molecules mediating volume transmission in the nervous system," *Frontiers in physiology*, vol. 3, pp. 319–319, 2012.
- [42] E. Del-Bel and F. F. De-Miguel, "Extrasynaptic neurotransmission mediated by exocytosis and diffusive release of transmitter substances," *Frontiers in synaptic neuroscience*, vol. 10, pp. 13:1–8, 2018.
- [43] B. Sarkar, A. K. Das, S. Arumugam, S. K. Kaushalya, A. Bandyopadhyay, J. Balaji, and S. Maiti, "The dynamics of somatic exocytosis in monoaminergic neurons," *Frontiers in physiology*, vol. 3, pp. 414:1–13, 2012.
- [44] K. S. Kits and H. D. Mansvelder, "Regulation of exocytosis in neuroendocrine cells: spatial organization of channels and vesicles, stimulus-secretion coupling, calcium buffers and modulation," *Brain Research Reviews*, vol. 33, no. 1, pp. 78–94, 2000.
- [45] C. Trueta, B. Méndez, and F. F. De-Miguel, "Somatic exocytosis of serotonin mediated by L-type calcium channels in cultured leech neurons," *The Journal of physiology*, vol. 547, no. Pt 2, pp. 405–416, 2003.
- [46] S. Barg, J. Galvanovskis, S. O. Göpel, P. Rorsman, and L. Eliasson, "Tight coupling between electrical activity and exocytosis in mouse glucagon-secreting alpha-cells," *Diabetes*, vol. 49, no. 9, pp. 1500–1510, 2000.
- [47] A. Verkhratsky, M. Matteoli, V. Parpura, J.-P. Mothet, and R. Zorec, "Astrocytes as secretory cells of the central nervous system: idiosyncrasies of vesicular secretion," *The EMBO journal*, vol. 35, no. 3, pp. 239–257, 2016.
- [48] V. Parpura, V. Grubii, and A. Verkhratsky, " Ca^{2+} sources for the exocytotic release of glutamate from astrocytes," *Biochimica et Biophysica Acta (BBA) - Molecular Cell Research*, vol. 1813, no. 5, pp. 984–991, 2011.
- [49] S. Nadkarni and P. Jung, "Modeling synaptic transmission of the tripartite synapse," *Physical Biology*, vol. 4, no. 1, pp. 1–9, 2007.

- [50] F. Mesiti, M. Veletic, P. A. Floor, and I. Balasingham, "Astrocyte-neuron communication as cascade of equivalent circuits," *Nano Communication Networks*, vol. 6, no. 4, pp. 183–197, 2015.
- [51] M. D'Ascenzo, M. Vairano, C. Andreassi, P. Navarra, G. B. Azzena, and C. Grassi, "Electrophysiological and molecular evidence of L-(Cav1), N-(Cav2.2), and R-(Cav2.3) type Ca^{2+} channels in rat cortical astrocytes," *Glia*, vol. 45, no. 4, pp. 354–363, 2004.
- [52] K. Dunlap, J. I. Luebke, and T. J. Turner, "Exocytotic Ca^{2+} channels in mammalian central neurons," *Trends in Neurosciences*, vol. 18, no. 2, pp. 89–98, 1995.
- [53] S. Bolton, K. Greenwood, N. Hamilton, and A. M. Butt, "Regulation of the astrocyte resting membrane potential by cyclic amp and protein kinase A," *Glia*, vol. 54, no. 4, pp. 316–328, 2006.
- [54] J. Sneyd, A. C. Charles, and M. J. Sanderson, "A model for the propagation of intercellular calcium waves," *American Journal of Physiology-Cell Physiology*, vol. 266, no. 1, pp. C293–C302, 1994.
- [55] S. Nadkarni and P. Jung, "Dressed neurons: modeling neural–glial interactions," *Physical Biology*, vol. 1, no. 1, pp. 35–41, 2004.